Direct RF Sampling Hyperspectral Microwave Radiometer (DSμRAD) for Ground Use

Takashi Maeda, *Senior Member, IEEE*, Noriyuki Kawaguchi, Ken-ichi Harada, Kensuke Ozeki, Yuichi Chikahiro, Hirofumi Onuki, Yoshinori Hayashi, Kenji Ema, Kazuhiro Naoki, Masashige Nakayama, and Tadashi Takano, *Life Fellow, IEEE*

***Abstract*— A microwave radiometer (MWR) is an instrument used to measure the microwave power emitted from the natural origin as a brightness temperature (T_B). A more active use of microwaves below the Ka-band is being planned for wireless communication in the near future, thereby increasing the risk of artificial radio frequency interference (RFI) with natural origin T_B measurement. Although measuring T_B values in high-frequency resolution is an effective way to detect and remove the effect of RFI from measured T_B, it is difficult to fundamentally increase the number of simultaneously measurable T_B in the conventional MWR due to space issues. Therefore, we developed a new MWR – direct RF sampling hyperspectral microwave radiometer (DSμRAD) that adopts multiple A/D converters of 10-GSPS order [samples per second (SPS)] to digitize microwave power received by an ultrawideband antenna. DSμRAD can measure the microwave power of the vertical and horizontal polarizations to decompose each into a T_B spectrum from 512 MHz to 40.96 GHz at 16-MHz intervals. We expect that DSμRAD will open up new possibilities for microwave remote sensing, including a drastic response to increased RFI risk, i.e., effective detection and removal (or extraction) of RFI. This letter presents the DSμRAD design in detail and the initial evaluation results of the instrument's performance.**

***Index Terms*— Antialiasing filter (AAF), flash A/D converter (ADC), quad-ridged feed horn (QRFH), ultrawide bandwidth, *Y*-factor method.**

I. Introduction

MICROWAVE passive remote sensing is a discipline that measures the microwave power radiated from every material and reveals its properties. A microwave radiometer (MWR) is an instrument that measures such a microwave power.

Manuscript received November 26, 2019; revised January 29, 2020, March 7, 2020, and April 14, 2020; accepted April 23, 2020. Date of publication June 3, 2020; date of current version May 21, 2021. *(Corresponding author: Takashi Maeda.)*

Takashi Maeda is with Satellite System Development Office, Japan Aerospace Exploration Agency (JAXA), Tsukuba 305-8505, Japan (e-mail: maeda.takashi@jaxa.jp).

Noriyuki Kawaguchi is with the National Astronomical Observatory of Japan (NAOJ), Mitaka 181-8588, Japan (e-mail: kawagu.nori@nao.ac.jp).

Ken-ichi Harada, Kensuke Ozeki, Yuichi Chikahiro, Hirofumi Onuki, Yoshinori Hayashi, and Kenji Ema are with Elecs Industry Co. Ltd., Kawasaki 213-0014, Japan (e-mail: harada@elecs.co.jp; ozeki@elecs.co.jp; chikahiro@elecs.co.jp; onuki@elecs.co.jp; hayashi@elecs.co.jp; ema@elecs.co.jp).

Kazuhiro Naoki is with the Research and Information Center, Tokai University, Tokyo 108-0074, Japan (e-mail: naoki.kazuhiro.k@tokai.ac.jp).

Masashige Nakayama is with the Graduate School of Education, Hokkaido University of Education, Kushiro Campus, Kushiro 085-8580, Japan (e-mail: nakayama.masashige@k.hokkyodai.ac.jp).

Tadashi Takano is with the Institute of Space and Astronautical Science (ISAS), Japan Aerospace Exploration Agency (JAXA), Sagamihara 252-5210, Japan (e-mail: ttakano@ac.jaxa.jp).

Digital Object Identifier 10.1109/LGRS.2020.2990707

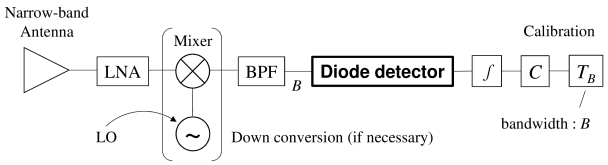

Fig. 1. Block diagram of a receiver in a total power (conventional) MWR.

Fig. 1 shows a block diagram of a receiver in a total power (conventional) MWR. Microwave power in a desired frequency band B (several 100 MHz to several gigahertz) is received by an antenna, amplified by a low noise amplifier (LNA), down-converted to intermediate frequency (IF) using a local oscillator (LO) and a mixer (if necessary), cut out by a bandpass filter (BPF), and detected by a diode. Then, the detected power is temporally integrated, with the obtained count value (C) being calibrated to the brightness temperature (T_B). Calibration is performed using a C–T_B curve obtained by actually measuring two or more objects believed to have known T_B values.

In a satellite-borne conventional MWR such as AMSR2 of JAXA [1], multifrequency T_B values from several gigahertz to several tens of gigahertz must be measured to retrieve various geophysical values. However, as the frequency interval between each T_B increases, an independent receiver set including an antenna (Fig. 1) must be installed for each T_B. Eventually, the number of receiver sets installable in the entire MWR (i.e., number of measurable T_B values) is at most limited to about ten due to space issues.

Furthermore, in the MWRs for ground use, an instrument based on the same concept as the satellite-borne MWR is large (e.g., RPG-DPR series of Radiometer Physics GmbH), and a small instrument can only measure the single frequency T_B (e.g., PR series of Radiometrics Corporation). Particularly, in ground observation, there may be a short distance to the observation target (only a few meters) as in the fixed-point observation of sea ice from the quay. In such a case, the space between the adjacent antennas of different receiver sets cannot be ignored with respect to the observation distance; consequently, reliably observing the same target at the same pointing and incident angles cannot be ensured.

Moreover, although the frequency band protected for microwave passive remote sensing is selected for the center frequency and bandwidth, the natural origin microwave power is weak. Even if the desired frequency band is filtered by the BPF, radio frequency interference (RFI) from any strong transmission source in the adjacent frequency band cannot be completely prevented from mixing into there. Once T_B is thus contaminated with RFI, it is difficult to restore the original T_B from there. The frequency band below the Ka-band (40 GHz)

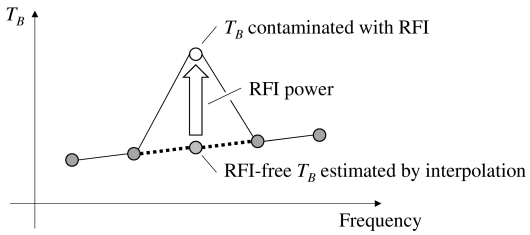

Fig. 2. Simple concept of RFI correction in T_B values measured in high-frequency resolution.

is expected to be used more actively in the near future, such as in 5G wireless communications, thereby raising concerns about microwave passive remote sensing becoming more difficult.

In general, RFI may occupy only a narrow bandwidth, and RFIs may be spread over a wide frequency range. T_B contaminated with RFI can be detected by measuring the continuous T_B values of the narrow bandwidth (i.e., hyperspectral T_B values) over such a frequency range. Fig. 2 shows the simple concept of RFI correction. According to Fig. 2, the original T_B is restored from that contaminated with RFI by linearly interpolating RFI-free T_B values in the adjacent frequency bins.

A conventional MWR for sounding measurement [2] is able to realize the concept, but the number of T_B values is still limited to several tens. Otherwise, it is conceivable to replace the diode detector of Fig. 1 with an A/D converter (ADC) and a fast Fourier transform (FFT) processor. When a received microwave signal is digitized at the sampling frequency F [samples per second (SPS), i.e., hertz] and N (powers of two) samples are processed by the FFT, the T_B spectrum is obtained. This T_B spectrum is composed of $N/2$ T_Bs whose B is F/N each, and eventually, the frequency range of the T_B spectrum is $F/2$.

Some existing satellite-borne (airborne) MWRs such as SMAP [3] and CubeRRT [4] (EMIRAD [5]) use this technique. However, the sampling frequency of the ADCs installed in SMAP and EMIRAD is 200 MSPS or less, so the frequency range of the T_B spectrum is restricted up to 100 MHz. On the other hand, in CubeRRT, the frequency of the LO of Fig. 1 is swept like a spectrum analyzer to extend the frequency range of the T_B spectrum, but a sweep of the frequency of LO takes time. For example, a microwave signal from 6 to 40 GHz is swept by the LO and decomposed to 34 IF signals with a 1-GHz range, and the T_B spectrum of each IF is measured by temporal integration of 100 ms [4]. Focusing on the specific 1-GHz IF block, its measurement interval becomes at least 3.4 s.

In order to solve the problems that existing MWRs could not overcome to address RFI, we have thus developed a new MWR [direct RF sampling hyperspectral microwave radiometer (DSμRAD)] that measures the T_B spectrum of 16-MHz intervals from 512 MHz to 40.96 GHz instantly. This letter presents the DSμRAD design in detail and the initial evaluation results of the instrument's performance.

II. DSμRAD

A. Appearance

Fig. 3 shows the appearance of DSμRAD. All of its components are guaranteed to operate above -20 °C for use in the field observations of sea ice in the polar regions, and

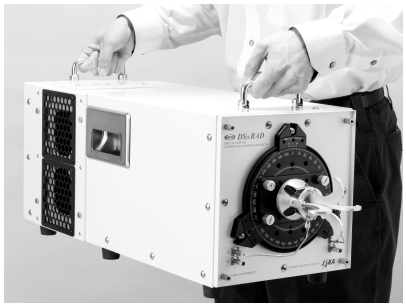

Fig. 3. Appearance of DSμRAD with a QRFH antenna.

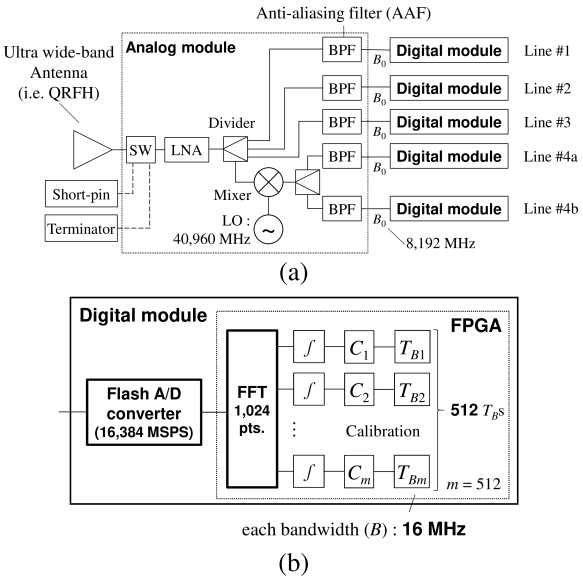

Fig. 4. Block diagram of DSμRAD. (a) Overall maximum configuration (SW: RF switch, LO: Local oscillator). (b) Each digital module when performing 1024-point FFT.

the instrument operates not only on 100–240 VAC but also on 12–32 VDC for battery drive. Measuring about 30 cm in both width and height and about 90 cm in depth, DSμRAD weighs around 20 kg and is installed on a large tripod.

The receiving antenna mounted to the front part is detachable, and an antenna optimal for the observation frequency range can be selected. In particular, we focused on the quad-ridged feed horn (QRFH) as an ultrawideband antenna. The QRFH has been studied as a radio astronomy feed horn [6] and can simultaneously receive the vertical and horizontal polarization components of ultrawideband microwave power. QRFHs covering the L- to K-bands and C- to Ka-bands are now commercially available. In Fig. 3, the QRFH (QH4000 of Microwave Vision Group Inc.) is installed. The QH4000 nominally covers the frequency range from 4 to 40 GHz. The goal of QRFH is to keep the gain (i.e., field of view (FOV) size) constant regardless of frequency, and the QH4000 FOV size can also be considered constant over a wider frequency range. To make the spatial resolution of T_B images with different FOV sizes identical, an FOV synthesis technique [1] can be applied.

B. High-Speed A/D Conversion

Fig. 4(a) shows the block diagram of DSμRAD in the maximum configuration to measure T_B of vertical or horizontal polarization. Microwave power received as voltage (hereinafter referred to as a received signal) by the QRFH is amplified by

TABLE I
FREQUENCY RANGE OF EACH LINE

Line	Nominal [MHz]			Recommended [MHz]		
#1	DC	$\leq f <$	8,192	512	$\leq f \leq$	7,920
#2	8,192	$< f \leq$	16,384	8,432	$\leq f \leq$	16,112
#3	16,384	$\leq f <$	24,576	16,640	$\leq f \leq$	24,352
#4a	24,576	$\leq f <$	32,768	24,848	$\leq f \leq$	32,528
	(16,384	$\geq f >$	8,192)*			
#4b	32,768	$< f \leq$	40,960	33,040	$\leq f \leq$	40,448
	(8,192	$> f \geq$	DC)*			

f : frequency, * as an IF

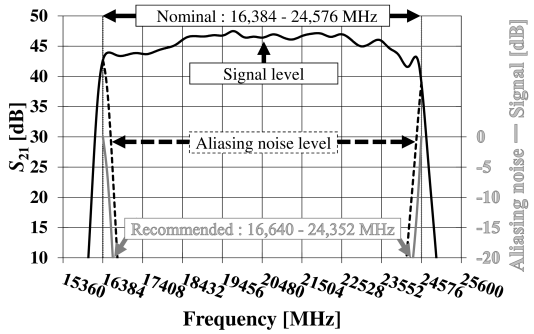

Fig. 5. Frequency pass characteristic (S_{21}) of the AAF on line #3.

an ultrawideband LNA (preamplifier) and distributed to four lines by a divider, and the received signal of each line is cut out with a bandwidth of 8192 MHz (B_0 in the figure) by the BPF. The number of lines can be flexibly adjusted according to user demand. Table I shows the frequency range of each line. This BPF on each line is specialized for the purpose of minimizing the aliasing noise that can occur in digitizing the received signal with an ADC located in the digital module at the subsequent stage and has a steep shoulder characteristic. Therefore, it is specifically called an antialiasing filter (AAF). The AAF on line #4a (#4b) has the same characteristics as that on line #2 (#1).

Fig. 4(b) shows a block diagram of the digital module following the AAF. The received signal extracted by the AAF with the bandwidth of 8192 MHz is digitized by the flash type ADC (HMCAD5831 of Analog Devices Inc.) with a sampling frequency of 16 384 MSPS. This ADC achieves the sampling frequency in the single A/D conversion circuit. On the contrary, a time interleave ADC realizes high-speed sampling by paralleling multiple low-speed A/D conversion circuits while shifting the clock, but it is difficult to keep accurate clock deviation between them [7], so it was not used. Each line can be turned on and off individually to save power, especially in battery drive. Either the digital module on line #4a or #4b can be selected for use.

As an example, Fig. 5 shows the frequency pass characteristic (S_{21}) of the AAF on line #3. Actually, the AAF (module) in DSμRAD has a built-in LNA, and S_{21} includes the gain of the LNA. The black solid line represents S_{21} of the original signal that passes through the AAF and follows the vertical axis on the left. Although the AAF has steep shoulder characteristics just below 16 384 MHz and just above 24 576 MHz, after A/D conversion, the frequency components outside the desired range (16 384–24 576 MHz) are folded into the inside of this range as indicated by the black dotted line in Fig. 5. The aliasing noise is such frequency components folded into the inside of the desired range due to A/D conversion. In DSμRAD, the ratio of aliasing noise to original signal (i.e., the difference between S_{21} values of the original signal and aliasing noise) is calculated for each frequency component. The ratio is indicated by the gray line in Fig. 5 and follows the vertical axis on the right. As a standard, the frequency range where the ratio is 1% (−20 dB) or less is defined as the recommended frequency range in Table I. In this example of line #3, the recommended frequency range is from 16 640 to 24 352 MHz. The lower limit (upper limit) of the recommended frequency range on line #1 (#4b) is 512 (40 448) MHz due to the high-pass filter (HPF) used for dc protection.

The fold of frequency components by an ADC is used skillfully in DSμRAD. The frequency range on each line is less than 8192 MHz, so according to the sampling theorem, the received signals not only on lines #1 and #4b but also on other lines are properly digitized. For example, on line #2, 8192–16 384 MHz is digitized as 8192 MHz–dc, and on line #3, 16 384–24 576 MHz is digitized as dc–8192 MHz. This means that the ADC functions as a frequency down converter. The frequency range of the received signal is from the L-band to the Ka-band (i.e., the frequency range over 40 GHz), but using this technique eliminates the need for an ADC with a sampling frequency of 80 GSPS.

C. Processing on FPGA (FFT and Temporal Integration)

The received signal digitized by the ADC in each digital module is decomposed into each frequency component by the subsequent FFT implemented on a field-programmable gate array (FPGA; the Kintex Ultrascale+ of Xilinx Inc.). The operation speed of the FPGA is much slower than that of the ADC used here but corresponds to the operating speed of the ADC in parallel processing.

In DSμRAD, 64, 128, 256, 512, or 1024 points can be selected as the number of FFT points. In case of the 1024-point FFT, the received signal is decomposed into 512 frequency components at 16-MHz intervals. It can be said that the smaller the interval, the higher the frequency resolution of the measurement. The FFT points entail a power of 2, and to make the frequency interval, an integer for the sake of convenience, the sampling frequency of the ADC should have been an integral multiple of a power of 2. Therefore, the sampling frequency of the ADC in DSμRAD was set to 16 384 (2^{14}) MSPS.

Next, the Fourier coefficient of each frequency component of the received signal is denoted as X (complex number). As mentioned at the beginning of this section, the substance of the received signal is the voltage received by the antenna. Therefore, XX^* (X^*: the complex conjugate of X) which represents the square of the voltage is proportional to the electrical power of the received signal (P).

Finally, XX^* is integrated within the integration time (τ) selected from 1, 10, 100, or 1000 ms, and a count value (C) corresponding to the bandwidth (B) of each frequency component is output. Since C is a product of XX^* ($\propto P$) and τ, it is proportional to the electrical energy of the received signal (E).

D. Calibration by Y-Factor Method

C corresponding to B of each frequency component is finally calibrated to T_B. Since $C \propto E$ as described in Section II-C, the relationship with T_B can be written as follows:

$$C \propto E\,[\mathrm{J}] \xrightarrow{/\tau} P\,[\mathrm{W}] \xrightarrow{/(kB)} T_B\,[\mathrm{K}] \tag{1}$$

where k is the Boltzmann's constant.

In the conventional MWR for ground use, C of a radio wave absorber or noise diode (ND) was measured as a calibration source with known T_B. The C–T_B curve was then constructed from the known relationship between C and T_B, and an arbitrary T_B was calibrated from the corresponding C using this curve. However, it is difficult to cool the radio wave absorber that can cover the whole QRFH used in DSμRAD with liquid nitrogen, and the ND characteristics vary with ambient temperature and aging. Constantly using the radio wave absorber or ND as a calibration source eventually reduces the maintainability of DSμRAD. Therefore, we have developed a method of calibrating T_B from C with the Y-factor method originally used for the noise figure measurements.

The Y-factor is the ratio of P when two different targets are measured. It can also be said that the Y-factor is the ratio of C by multiplying the numerator and denominator by τ from the relationship of (1). If C_{I} and C_{II} are obtained by measuring targets I and II, their Y-factor is defined as

$$Y \equiv \frac{C_{\mathrm{I}}}{C_{\mathrm{II}}}. \tag{2}$$

If C_{I} (C_{II}) is measured for a frequency component with bandwidth B and the gain of the entire analog module (system gain) is denoted as G_{I} (G_{II}), (2) can be rewritten as

$$Y = \frac{G_{\mathrm{I}}(kBT_{B\mathrm{I}} + kBT_r)\tau}{G_{\mathrm{II}}(kBT_{B\mathrm{II}} + kBT_r)\tau} \tag{3}$$

where $T_{B\mathrm{I}}$ ($T_{B\mathrm{II}}$) is T_B of the frequency component of target I (II), and T_r is the receiver noise temperature emitted from the entire analog module. Furthermore, if the measurement time difference between C_1 and C_2 is small enough, it can be regarded as $G_{\mathrm{I}} = G_{\mathrm{II}} \equiv G$, and (3) is finally simplified to

$$Y = \frac{T_{B\mathrm{I}} + T_r}{T_{B\mathrm{II}} + T_r}. \tag{4}$$

Thus, the Y-factor method has the advantage of removing the effects of system gain fluctuation from the calibration process.

In Fig. 4(a), an RF switch is installed between the antenna and the LNA. The input of the LNA can be switched to a terminator or a short pin (i.e., metal terminal cap), as well as to the antenna. Since the microwave power input to the terminator is almost completely absorbed, its emissivity (e) can be regarded as 1, and the physical temperature of the terminator (T_{term}) is thus treated as T_B. T_{term} is measured by a platinum temperature sensor attached to the terminator.

Moreover, regarding the noise of the entire analog module (N), N is caused by a random electron motion from the source to the drain through the gate of the transistor in the LNA. Therefore, N is emitted not only to the output side (between the drain and source) as T_r but also to the input side (between the gate and source) of the LNA. Based on this concept, the short pin is intended to completely reflect N emitted from the input side of the LNA so that N is used as the input of the LNA. Accordingly, T_B when measuring the short pin is proportional to T_r and can be written as αT_r. Since α is determined by the circuit configuration, it is considered to hardly change. The verification result of the stability of α will be described in another paper or letter.

First of all, C values of the terminator and the short pin (C_{term} and C_{short}) are obtained. Then, their Y-factor (Y_{ts}) is defined as follows:

$$Y_{\mathrm{ts}} \equiv \frac{C_{\mathrm{term}}}{C_{\mathrm{short}}} = \frac{T_{\mathrm{term}} + T_r}{(\alpha + 1)T_r}. \tag{5}$$

As a result, the unknown T_r is obtained as

$$T_r = \frac{T_{\mathrm{term}}}{(\alpha + 1)Y_{\mathrm{ts}} - 1}. \tag{6}$$

Next, using C values of the terminator and the environment (observed via the antenna) (C_{term} and C_{ant}), another Y-factor (Y_{ta}) is defined as

$$Y_{\mathrm{ta}} \equiv \frac{C_{\mathrm{term}}}{C_{\mathrm{ant}}} = \frac{T_{\mathrm{term}} + T_r}{T_{\mathrm{ant}} + T_r}. \tag{7}$$

As T_r is already obtained in (6), T_B of environment (T_{ant}) is calculated by a modification of (7) as

$$T_{\mathrm{ant}} = \frac{T_{\mathrm{term}} + T_r}{Y_{\mathrm{ta}}} - T_r. \tag{8}$$

Thus, C_{ant} is calibrated to T_{ant}. T_r is obtained from (6) at each time interval, where T_r cannot be considered as a constant. The time interval depends on the variation of ambient temperature.

In DSμRAD, the linearity between C and T_B was confirmed from 80 to 1200 K. For T_B lower than ambient temperature, a radio wave absorber immersed in liquid nitrogen was observed. For T_B higher than ambient temperature, the corresponding noise was input by an ND attached instead of the antenna.

As shown in Fig. 4(a), DSμRAD uses an ultrawideband LNA covering 512 MHz–40.96 GHz as a preamplifier, and the noise temperature of the preamplifier is nominally about 1000 K. However, the other components of the analog module were selected so that the radiometric resolution (ΔT) of T_{ant} is typically 0.75 K or less when measuring a radio wave absorber with constant T_B (300 K) under the conditions of ambient temperature (300 K), $B = 16$ MHz, and $\tau = 1$ s. This ΔT is comparable to nominal ΔT values of the conventional MWRs for ground use described in Section I.

α is obtained by connecting a calibrated ND instead of the antenna at factory shipment or periodic inspection of DSμRAD. For the calibrated ND, an excess noise ratio (ENR) is given for each frequency component as

$$\mathrm{ENR} \equiv \frac{T_{\mathrm{up}} - T_{\mathrm{down}}}{T_0} \tag{9}$$

where $T_0 = 290$ K, and T_{up} (T_{down}) is T_B of noise output from the ND with the power on (off). Besides C_{term} and C_{short}, when C_{up} and C_{down} are measured for the ND with the power on and off, the Y-factors defined by the following equations are obtained:

$$Y_{\mathrm{ut}} \equiv \frac{C_{\mathrm{up}}}{C_{\mathrm{term}}} = \frac{T_{\mathrm{up}} + T_r}{T_{\mathrm{term}} + T_r} \tag{10}$$

$$Y_{\mathrm{ts}} \equiv \frac{C_{\mathrm{term}}}{C_{\mathrm{short}}} = \frac{T_{\mathrm{term}} + T_r}{(\alpha + 1)T_r} \tag{11}$$

$$Y_{\mathrm{dt}} \equiv \frac{C_{\mathrm{down}}}{C_{\mathrm{term}}} = \frac{T_{\mathrm{down}} + T_r}{T_{\mathrm{term}} + T_r}. \tag{12}$$

As there are four unknowns (T_{up}, T_{down}, T_r, and α) in the four equations [see (9)–(12)], this simultaneous equation can be solved. In particular, α of the frequency component is obtained as

$$\alpha = \frac{\mathrm{ENR} \cdot T_0}{Y_{\mathrm{ts}}\{\mathrm{ENR} \cdot T_0 - (Y_{\mathrm{ut}} - Y_{\mathrm{dt}}) \cdot T_{\mathrm{term}}\}} - 1. \tag{13}$$

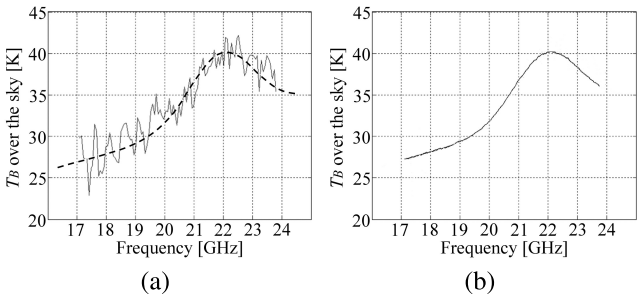

Fig. 6. T_B spectrum of the sky measured by line #3 for vertical polarization. (a) T_B spectrum obtained in the first integration time slot ($T_{B0}(f)$; black solid line) and the RTM regressed to $T_{B0}(f)$ ($M(f)$; black dotted line). (b) T_B spectrum obtained in the subsequent integration time slot with reduced ripple. ($T'_{Bn}(f)$).

III. Performance Evaluation

Fig. 6 shows the T_B spectrum measured by line #3 when the sky was actually observed with DSμRAD. The sky was clear during this observation, and the elevation of DSμRAD was 90°. There were 1024 FFT points, and the integration time was 1000 ms. Lines other than #3 were turned off. Fig. 6(a) shows a T_B spectrum in the first integration time slot by using the black solid line. It is denoted as $T_{B0}(f)$ (f: frequency at 16-MHz intervals). $T_{B0}(f)$ is varying rapidly as a function of frequency, here denoted ripple. Ripple indicates that the microwave signals are partly reflected at each contact between components in the analog modules shown in Fig. 4(a) due to impedance mismatch, thus causing standing waves that increase or decrease the signal levels of particular frequencies at the output of the analog modules. Attenuators and isolators are incorporated in the analog modules to suppress the generation of standing waves as much as possible but are omitted in Fig. 4(a). Nevertheless, it is difficult to completely suppress ripple. Conversely, by observing the T_B spectrum with DSμRAD, it can be said that the ripple latent in conventional MWR measurements has been clearly visualized.

Such a ripple is reduced by software processing in DSμRAD. As mentioned above, if ripple is caused by reflections at the contacts between components in an analog module, the location of the contacts (i.e., reflection points) is fixed. Accordingly, the electrical length from the output end of the analog module to each reflection point and, eventually, the period of the ripple in the frequency direction are considered not to fluctuate. Based on such assumption for the ripple, $T_{B0}(f)$ is first regressed to a polynomial of the fourth or fifth order ($M(f)$), and the ripple pattern ($R(f)$) is extracted as

$$R(f) = T_{B0}(f) - M(f). \tag{14}$$

Next, subtracting $R(f)$ extracted in this way from the T_B spectrum obtained in the subsequent integration time slot ($T_{Bn}(f)$) yielded the T_B spectrum with reduced ripple ($T'_{Bn}(f)$). That is

$$T'_{Bn}(f) = T_{Bn}(f) - R(f). \tag{15}$$

If a radiative transfer model (RTM) is known, $M(f)$ may be created using the RTM. Actually, $M(f)$ indicated by the black dotted line in Fig. 6(a) was created the RTM by Shambayati [8]. $T'_{Bn}(f)$ in Fig. 6(b) was obtained 1 min after $T_{B0}(f)$. The increase of T_B due to the resonance of water vapor was clearly visualized around 21–23 GHz in $T'_{Bn}(f)$. If $T'_{Bn}(f)$ in each integration time slot is fitted to the RTM, it is possible to retrieve the temporal variations in the amount of water vapor and liquid water. However, it should be noted that if a known RTM is used as $M(f)$, any deviation from the known RTM may be recognized as a ripple.

Importantly, once determined, $R(f)$ was reusable for a few minutes, and the system gain was considered constant. Consequently, it was confirmed that the assumption for the ripple is correct.

IV. Conclusion

DSμRAD is the world's first ultrawideband hyperspectral MWR that can measure the microwave power of vertical and horizontal polarizations received by a QRFH antenna to decompose each into a T_B spectrum from 512 MHz to 40.96 GHz at 16-MHz intervals. By DSμRAD, it is possible to select T_B values of optimum frequencies according to the geophysical values to be retrieved. Besides, expanding the use of MWRs, such as for investigating RFI sources in the environment, is also expected. We first developed DSμRAD for ground use but will continue the study so that the knowledge gained here will become the cornerstone of future satellite-borne MWRs. At the same time, we hope to spread DSμRAD as a low-cost, general-purpose MWR that meets the broad requirements of the MWR community.

References

[1] T. Maeda, K. Imaoka, and Y. Taniguchi, "GCOM-W1 AMSR2 Level 1R product: Dataset of brightness temperature modified using the antenna pattern matching technique, *IEEE Trans. Geosci. Remote Sens.*, vol. 54, no. 2, pp. 770–782, Feb. 2016, doi: 10.1109/TGRS.2015.2465170.

[2] R. Ware *et al.*, "A multichannel radiometric profiler of temperature, humidity, and cloud liquid," *Radio Sci.*, vol. 38, no. 4, p. 8079, Aug. 2003, doi: 10.1029/2002RS002856.

[3] D. Bradley *et al.*, "Radio-frequency interference (RFI) mitigation for the soil moisture active/passive (SMAP) radiometer," in *Proc. IEEE Int. Geosci. Remote Sens. Symp. (IGARSS)*, Jul. 2010, pp. 2015–2018, doi: 10.1109/IGARSS.2010.5652482.2010.

[4] S. Misra *et al.*, "The cubesat radiometer radio frequency interference technology (CubeRRT) validation mission: Performance and development of the digital backend technology," in *Proc. IEEE Int. Geosci. Remote Sens. Symp. (IGARSS)*, Jul. 2017, pp. 1—4, doi: 10.1109/IGARSS.2017.8127187.2017.

[5] S. S. Søbjærg, S. S. Kristensen, J. E. Balling, and N. Skou, "The airborne EMIRAD L-band radiometer system," in *Proc. IEEE Int. Geosci. Remote Sens. Symp. (IGARSS)*, Jul. 2013, pp. 1900–1903, doi: 10.1109/IGARSS.2013.6723175.2013.

[6] V. Rodriguez, "A multi-octave, open-boundary, quad-ridge horn antenna for use in the S-to Ku-bands," *Microw. J.*, vol. 49, no. 3, pp. 84–92, 2006.

[7] N. Kurosawa, H. Kobayashi, K. Maruyama, H. Sugawara, and K. Kobayashi, "Explicit analysis of channel mismatch effects in time-interleaved ADC systems," *IEEE Trans. Circuits Syst. I, Fundam. Theory Appl.*, vol. 48, no. 3, pp. 261–271, Mar. 2001, doi: 10.1109/81.915383.2001.

[8] S. Shambayati, "Atmosphere attenuation and noise temperature at microwave frequencies," in *Low-Noise Systems in the Deep Space Network*, M. S. Reid, ed. Hoboken, NJ, USA: Wiley, 2008, ch. 6.